Toll-like receptor 4 promotes bladder cancer progression upon S100A8/A9 binding, which requires TIRAP-mediated TPL2 activation

Acosta Gonzalez Herik Rodrigo[a,b,1], Nahoko Tomonobu[a,1], Haruka Yoneda[a], Rie Kinoshita[a], Yosuke Mitsui[b], Takuya Sadahira[b], Shin-ichi Terawaki[c], Yuma Gohara[a], Ni Luh Gede Yoni Komalasari[a,h], Fan Jiang[a], Hitoshi Murata[a], Ken-ichi Yamamoto[a], Junichiro Futami[d], Akira Yamauchi[e], Futoshi Kuribayashi[e], Yusuke Inoue[c], Eisaku Kondo[f,i], Shinichi Toyooka[g], Masahiro Nishibori[a], Masami Watanabe[b], Yasutomo Nasu[b], and Masakiyo Sakaguchi[a*]

[a]Department of Cell Biology, Okayama University Graduate School of Medicine, Dentistry and Pharmaceutical Sciences, Okayama, Japan.

[b]Department of Urology, Okayama University Graduate School of Medicine, Dentistry and Pharmaceutical Sciences, Okayama, Japan.

[c]Faculty of Science and Technology, Division of Molecular Science, Gunma University, Kiryu, Gunma, Japan.

[d]Department of Interdisciplinary Science and Engineering in Health Systems, Okayama University, Okayama, Japan.

[e]Department of Biochemistry, Kawasaki Medical School, Kurashiki, Okayama, Japan.

[f]Division of Molecular and Cellular Pathology, Niigata University Graduate School of Medical and Dental Sciences, Niigata, Japan.

[g]Department of General Thoracic Surgery and Breast and Endocrinological Surgery, Okayama University Graduate School of Medicine, Dentistry and Pharmaceutical Sciences, Okayama, Japan.

[h]Faculty of Medicine, Udayana University, Denpasar, Bali, Indonesia.

[i]Division of Tumor Pathology, Near InfraRed Photo-Immuno-Therapy Research Institute, Kansai Medical University, Osaka, Japan.

[1]These authors contributed equally to this work.

[*]Corresponding author: Masakiyo Sakaguchi

E-mail: masa-s@md.okayama-u.ac.jp

Phone number: +81-86-235-7395; Fax: +81-86-235-7400

Abstract

Bladder cancer is an often widely disseminated and deadly cancer. To block the malignant outgrowth of bladder cancer, we must elucidate the molecular-level characteristics of not only bladder cancer cells but also their surrounding milieu. As part of this effort, we have long been studying extracellular S100A8/A9, which is elevated by the inflammation associated with certain cancers. Extracellularly enriched S100A8/A9 can hasten a shift to metastatic transition in multiple types of cancer cells. Intriguingly, high-level S100A8/A9 has been detected in the urine of bladder-cancer patients, and the level increases with the stage of malignancy. Nonetheless, S100A8/A9 has been investigated mainly as a potential biomarker of bladder cancers, and there have been no investigations of its role in bladder-cancer growth and metastasis. We herein report that extracellular S100A8/A9 induces upregulation of growth, migration and invasion in bladder cancer cells through its binding with cell-surface Toll-like receptor 4 (TLR4). Our molecular analysis revealed the TLR4 downstream signal that accelerates such cancer cell events. Tumor progression locus 2 (TPL2) was a key factor facilitating the aggressiveness of cancer cells. Upon binding of S100A8/A9 with TLR4, TPL2 activation was enhanced by an action with a TLR4 adaptor molecule, TIR domain-containing adaptor protein (TIRAP), which in turn led to activation of the mitogen-activated protein kinase (MAPK) cascade of TPL2. Finally, we showed that sustained inhibition of TLR4 in cancer cells effectively dampened cancer survival in vivo. Collectively, our results indicate that the S100A8/A9-TLR4-TPL2 axis influences the growth, survival and invasive motility of bladder cancer cells.

Key words: Bladder cancer, S100A8/A9, TLR4, TPL2

1. Introduction

S100A8/A9 is a heterodimer complex composed of S100A8 and S100A9 proteins, and is highly induced and present extracellularly at a high level in the cancer inflammatory milieu. A growing body of evidence indicates that S100A8/A9 activates cancer metastasis for several different cancers, including melanomas, breast cancers and lung cancers [1]. Efforts to identify the S100A8/A9 receptors involved in the activation of cancer cells and resulting cancer metastasis have yielded several important candidate receptors. These include Toll-like receptor 4 (TLR4) [2], receptor for advanced glycation endproducts (RAGE) [3], melanoma cell adhesion molecule (MCAM), activated leukocyte cell adhesion molecule (ALCAM), extracellular matrix metalloproteinase inducer (EMMPRIN) and neuroplastin-β (NPTNβ) [1]. Interestingly, each of these receptors is expressed in different cancer types, and the levels of expression correspond to the malignant grades, implying that these receptors function either singly or cooperatively depending on the cancer.

Bladder cancer generally originates in the urinary tract, and its worldwide incidence is estimated at 500,000 new cases and 200,000 deaths annually [4]. Several risk factors, such as a smoking habit, aging, exposure to specific chemicals used in the manufacture of dyes, and the parasitic infection known as schistosomiasis, have been suspected to contribute to the incidence of this type of cancer [5,6]. Of note, all the risk factors are closely associated with inflammation in a sustained manner. As mentioned above, the chronic inflammation milieu surrounding the sprouted bladder cancer may shift it towards greater aggression, and the inflammation-induced S100A8/A9 may make a major contribution to this shift. Indeed, high levels of S100A8/A9 have been detected in the urine of patients with bladder cancer, and these levels have been found to increase with the stage of malignancy [7]. However, the mechanism underlying the role of S100A8/A9 in the shift to a more malignant phenotype of bladder cancer has not been fully elucidated. Therefore, in this study, we aimed to clarify the role of S100A8/A9 in bladder cancer.

2. Materials and Methods

2.1 Cell lines and reagents

All cells and their cultured media used in this study were listed in Table S1. To selectively inhibit intrinsic kinase activities of TPL2, we used a TPL2 inhibitor (Cayman Chemical, Ann Arbor, MI). The TLR4-mediated signal transduction was suppressed by using a TLR4 inhibitor (Resatorvid; Selleck Bio-Tech, Osaka, Japan) or TIRAP inhibitor (Cell-permeable TIRAP inhibitor peptide; Merck Millipore, Kenilworth, NJ).

2.2 Plasmid vector

The cDNAs located on the multi-cloning site of the pIDT-SMART (C-TSC) vector [8] were all designed to be expressed in a C-terminal 3Flag-6His-tagged, 3Myc-6His-tagged or 3HA-6His-tagged form.

2.3 Recombinant proteins

The highly purified human recombinant S100A8/A9 heterodimer was prepared as described previously [9]. The glutathione transferase (GST)-fusion proteins were also prepared as previously reported [10]. In brief, cDNA of the human MEK1 kinase-dead (KD) form (a point mutation: K97M) was cloned into the pGEX6P1 vector (GE Healthcare, Chicago, IL). The cloned pGEX6P1 vector was transduced into Escherichia coli (E. coli), and the expressed product was purified using Glutathione Sepharose™ 4 Fast Flow (GE Healthcare). The GST-TIRAP fusion protein was obtained from Abnova (Taipei, Taiwan).

2.4 Immunohistochemistry (IHC)

A human bladder cancer tissue section microarray (US Biomax, Inc, Rockville, MD) was deparaffinized, and antigen retrieval was performed by conventional microwave treatment using a citric acid solution. The slides were then incubated with primary antibodies (Table S2) and followed a horseradish peroxidase (HRP)-labeled secondary antibody. Signals were visualized by treating the antibody-reacted slides with a substrate, 3,3′-Diaminobenzidine (DAB) (Vector, Burlingame, CA).

2.5 Real-time quantitative reverse transcription PCR (RT-qPCR)

Cultured cells were washed with phosphate-buffered saline, and total RNA was extracted using ISOGEN II Isolation Reagent (Nippon Gene, Tokyo). Then reverse-transcription was performed using ReverTraAce qPCR RT Master Mix with gDNA Remover (Toyobo, Osaka, Japan). RT-qPCR was performed using FastStart SYBR Green Master (Roche Applied Science, Penzberg, Germany) with specific primers (Table S3) on a LightCycler 480 system II (Roche Applied Science).

2.6 Cell-based assays in culture

A CellTiter 96® AQueous One Solution Cell Proliferation Assay (MTS) (Promega Biosciences) was used for the assessment of cell proliferation. Cells (1×10^4 cells) in 96-well plates were treated with lipopolysaccharide (LPS) (Santa Cruz Biotechnology) to a final

concentration of 100 ng/ml or S100A8/A9 recombinant protein to a final concentration of 1 μg/ml for one day. Cellular migration and invasion were evaluated by a Boyden chamber assay with a Matrigel-coated (for invasion) or non-coated (for migration) transwell membrane filter insert (pore size, 8 μm) in a 24-well plate (BD Biosciences, Franklin Lakes, NJ). Cells (3×10^4 cells/insert) were seeded with serum-free DMEM/F12 medium on the top chamber, and the bottom chamber was filled with DMEM/F12 medium containing 10% FBS. LPS or S100A8/A9 was then set in the bottom chamber at a final concentration of 100 ng/ml for LPS and 1 μg/ml for S100A8/A9. After incubation for 24 h, cells that passed through the filter were counted by staining with 0.01% crystal violet in 25% methanol. Migrated/invaded cells were microscopically imaged and quantified by cell counting in five non-overlapping fields at ×100 magnification. The numbers of migrated/invaded cells are presented as the average from three independent experiments.

2.7 Immunoprecipitation (IP)

Monoclonal anti-DYKDDDDK tag agarose (clone 1E6; Fujifilm Wako Pure Chemical, Osaka, Japan) and monoclonal anti-HA tag agaroses (Sigma-Aldrich) were used for the IP experiments to capture the ectopically overexpressed proteins. The tag-agarose beads were mixed with various cell extracts and incubated for 3 h at 4ºC. After incubations of the individual samples, the bound proteins were pulled down by centrifugation.

IP of endogenous proteins was also investigated using an avidin-biotin interaction as previously reported [11]. Rabbit anti-human TLR4 (Imgenex, San Diego, CA) and rabbit human anti-MEK2 antibody (Cell Signaling Technology) were biotinylated using a Biotin Labeling Kit-SH (Dojindo Molecular Technologies, Kumamoto, Japan) to recover antibody-free samples after IP using streptavidin-agarose (Thermo Fisher Scientific).

2.8 Western blotting (WB)

WB analysis was performed under conventional conditions [12]. The antibodies used were listed in Table S4.

2.9 Kinase reaction in a cell-free system

The in vitro kinase reaction was performed as reported previously with some modifications [13]. Briefly, 10 ng of each prepared recombinant protein and the pulled-down TPL2 specimen (10 ng) were mixed in a kinase buffer (50 mM Hepes/pH 7.4, 5 mM $MgCl_2$, 1 mM DTT, PhosphoSTOP (Roche Applied Science), protease inhibitor cocktail (Roche Applied Science) and 5 μM adenosine triphosphate (ATP)) to a total volume of 20 μl in a PCR tube. The mixed specimens were then incubated at 25°C for either 10 min or 60 min.

2.10 In vivo tumor model

J82 cells (6 x 10^6 cells) were subcutaneously transplanted into female NOD/SCID mice (Charles River Laboratories Japan Inc., Yokohama, Japan). Four mice were examined in each group. To selectively inhibit the TLR4-mediated signal in vivo, we used the same dose of TLR4 inhibitor as used in the report of Hua et al. [14]. The size of tumors was measured with a vernier caliper, and tumor volume was calculated as 1/2 × (shortest diameter)^2 × (longest diameter). In addition, excised tumors in all animal experiments were embedded in paraffin and sectioned, and then the sections were histologically examined by immunohistochemistry using antibodies (Table S2), and terminal deoxynucleotidyl transferase (TdT)-mediated dUTP nick-end labeling (TUNEL) staining.

2.11 Statistical analysis

Data are expressed as means ± standard deviation (SD). We used a simple pair-wise comparison with Student's *t*-test. Values of $p<0.05$ were considered statistically significant.

3. Results

3.1. Expression of S100A8/A9 and its receptors in bladder cancer

The macroscopic observation of the staining of the tissue microarray (Fig. S1A) showed that both the S100A8 and S100A9 levels in cancer tissues were higher than those in normal tissues, and the number of cases with elevated S100A8/A9 seemed to be higher among patients with advanced stage III cancers (Fig. S1B and S1C, left panel). The enlarged images of the sections also revealed that both S100A8 and S100A9 were upregulated in the bladder cancer lesions at stage III in comparison to those in normal bladder tissues ((Fig. S1B and S1C, right panel). Several specific receptors were available to the extracellular S100A8/A9, including both classical receptors (RAGE, TLR2, and TLR4) and novel receptors (MCAM, ALCAM, EMMPRIN, and NPTNα and β) [1], and we investigated their expression further to clarify their potential role in bladder cancer. RT-qPCR analysis revealed that one of these receptors, TLR4, was markedly elevated similarly in the two transitional bladder cancer cell lines, J82 and TCCSUP, compared to its expression in normal OUMS-24 fibroblasts and non-cancerous HEK293T cells (Fig. 1A). High-level elevation of TLR4 expression in bladder cancer cells was also observed when compared to the levels in normal HUC and immortal SV-HUC-1 cells (Fig. 1B). In line with this result, we also found that RAGE and MCAM were elevated in J82 and TCCSUP cells in a

consistent manner. Gathering the qPCR results from Fig. 1A and 1B, we decided to focus on TLR4 as a putative major S100A8/A9 receptor in bladder cancer cells. The high expression of TLR4 in bladder cancer cells was further confirmed by immunohistochemistry. The levels of TLR4 expression tended to be higher in all bladder cancer tissues compared to normal tissues (Fig. 1C, left panel), and these results were similar to the S100A8/A9 staining patterns in the same tissue arrays (Fig. S1B and S1C). Microscopic examination revealed an increased expression of TLR4 in the cancer lesions (Fig. 1C, right panel).

3.2. Role of S100A8/A9-TLR4 in bladder cancer cells

To further investigate the role of the upregulation of both S100A8/A9 and TLR4 in bladder cancer, we stimulated J82 cells with the purified recombinant S100A8/A9 or LPS, a major ligand for TLR4 [15]. Based on a report in which the average urinary levels of S100A8/A9 in patients with muscle-invasive bladder cancer were approximately 1 μg/ml [7], we stimulated J82 cells with 1 μg/ml of S100A8/A9. The stimulation induced the growth and migration of the cells (Fig. 1D and 1E). Because ERK activation is involved in these cellular events in bladder cancer cells [16], we studied the ERK condition in the treated cells. Using a WB analysis, we found that S100A8/A9 induced ERK phosphorylation that is required for an increase in the enzymatic activity of ERK, with the result that the levels of the ERK phosphorylation were elevated in a time-dependent manner, with a pattern similar to that of the LPS used as a positive control. A culture duration of 30 min was required to achieve the maximum levels of phosphorylation after the stimulation with both ligands (Fig. 1F). We next stimulated the cancer cells with different doses of S100A8/A9 at around 1 μg/ml for 30 min. The results showed that S100A8/A9 at doses of 1 and 10 μg/ml induced a marked activation of ERK (Fig. 1G). Interestingly, the 30-min stimulation with 1 μg/ml of S100A8/A9 and LPS (0.1 μg/ml) did not induce any appreciable alteration of phosphorylation of any effector kinases except ERK in J82 cells (Fig. 1H). These results drew our attention to the molecular mechanism by which TLR4 induces ERK activation upon the binding of the ligands in bladder cancer cells.

Because MAPKKKs are located at almost the top of the MAPK activation cascades (Fig. S2A), some MAPKKKs would be expected to associate with TLR4 just beneath the plasma membrane, which would cause the ERK activation cascade to be switched on in the presence of ligands. To investigate this potential series of events, we performed an interaction screening of MAPKKKs with TLR4. To detect potential interaction(s) between MAPKKKs and TLR4, we overexpressed the individual MAPKKKs-3Myc-6His as indicated in the image (Fig. S2B, left panel) with TLR4-3Flag-6His in HEK293T cells, and immunoprecipitated for the TLR4-3Flag-6His by using anti-DYKDDDDK tag agarose beads that recognize Flag tag. The co-precipitated MAPKKKs were then detected by WB using an anti-myc antibody. Of note, many MAPKKKs, including TAK1,

DLK, TPL2, ASK1, ARAF, and MOS, that were stained red were associated with TLR4 at different levels (Fig. S2B, left panel). To further examine these positive interactions, we then used the same method to investigate the interactions of these MAPKKKs with the major adaptor molecules of TLR4, TIRAP, MyD88, and TRAM. By this approach, we found that all of the stained MAPKKKs except for ASK1 effectively interacted with TIRAP (Fig. S2B, right panel). To determine the actual significance of the MAPKKKs that function dominantly in the presence of TLR4 in bladder cancer cells, we investigated the expression levels of these MAPKKKs. We found that TPL2 alone was remarkably upregulated in the two bladder cancer cell lines consistently (Fig. 2A). These results suggested that TPL2 functions as the dominant MAPKKK functioning in the presence of TLR4 to trigger the ERK1/2 activation cascade in bladder cancer cells upon the binding with ligands (Fig. 2B). To confirm this, a plasmid construct carrying TPL2 kinase-dead (KD) (a point mutation: K167M) was transfected to J82 cells to overexpress the foreign TPL2 KD that hides the proper function of intrinsic TPL2. It turned out that the LPS-mediated enhancements for growth, migration, and invasion were all nearly completely diminished by the TPL2 KD overexpression (Fig. 2C). We then found that a selective inhibitor of TPL2 abrogated these LPS-induced and S100A8/A9-induced enhancements in J82 cells (Fig. 2D). Similar results were also observed by exploiting the cell-permeable TIRAP inhibitor peptide (Fig. 2E). These results indicate that TPL2 plays a crucial rule in TLR4/TIRAP-derived cancerous cellular activities in bladder cancer cells.

3.3. Activation of TPL2 under TLR4

To examine the significance of TIRAP binding with TPL2 for the activation of TPL2, we prepared GST-fusion recombinant proteins (Fig. S3A). GST-MEK1 was selected as a suitable substrate for TPL2 on the TPL2-mediated MAPK cascade (Fig. S3B). To avoid a MEK1-derived phosphorylation reaction in the test tube, MEK1 was transformed to its MEK1 kinase-dead (KD) form (a point mutation: K97M). As described above, we faced a difficult challenge in realizing the expression and purification of TPL2 in the E. coli expression system that is employed for the GST fusion proteins. To overcome this problem, we expressed the TPL2 wild (WT) and KD types in HEK293T cells, and the resulting cells were lysed and the expressed foreign products were pulled-down (Fig. S3B and S3C). The individual pulled-down specimens included TPL2 WT and KD, respectively, and both were slightly contaminated with the bound intrinsic TIRAP for the TPL2 WT and KD (Fig. S3D). These prepared proteins were then mixed in a test tube and evaluated for the TPL2-mediated MEK1 phosphorylation by WB using an anti-phospho-serine/threonine antibody and anti-phospho-MEK1/2 (Ser218/222) antibody, whose phosphorylation-recognition sites are important for the activation of MEK1/2. As shown in Fig. 3A, phosphorylation was detected by both antibodies for GST-MEK1 KD, but not GST and GST-

TIRAP at the 10-min incubation and the reaction was further enhanced by an extended 60 min. We confirmed that the reaction was almost completely suppressed by the presence of a TPL2 inhibitor. The result was further confirmed by a similar experiment exploiting TPL2 KD, except that a TPL2 inhibitor was not used (Fig. 3B). In addition, the TPL2-mediated phosphorylation of MEK1 further increased along with the increasing doses of GST-TIRAP but not GST in the reaction mixture (Fig. 3C). These results indicate that TIRAP leverages TPL2 for its activation via their mutual interaction.

To consolidate the results, we next evaluated the learned molecular logic in bladder cancer cells by employing IP for detection of the TLR4-TIRAP-TPL2 interaction and MEK phosphorylation, and standard WB of whole cell lysates for the detection of ERK phosphorylation. As shown in Fig. 3D, we found that the TLR4 ligands, LPS and S100A8/A9, both induced recruitment of TIRAP and TPL2 to TLR4 and elevation of the phosphorylation of MEK2 and ERK1/2 in J82 cells, and these actions were significantly suppressed by the treatment with TPL2 inhibitor. Similar results were also confirmed in other TCCSUP cells (Fig. S4A). These results strongly indicate the presence of TPL2 on the TLR4 downstream pathway in bladder cancer cells, which leads to the activation of ERK through the TIRAP binding upon stimulation with the ligands.

3.4. Inhibitory effect of TLR4 on bladder cancer in vivo

To assess the significance of TLR4 in bladder cancer in vivo, we used a well-established tumor outgrowth mouse model of subcutaneously engrafted J82 cells. To inhibit the TLR4-mediated signal in J82 cells in vivo, a selective inhibitor of TLR4 named Resatorvid was intraperitoneally injected to the mice on the 6th day after the J82 transplantation, and every other day thereafter. This treatment induced a reduction of both tumor volume (Fig. 4A) and weight (Fig. 4B). These differences were more obvious on the interior than the exterior of the tumors (Fig. 4C)—that is, in the drug-treated tumors, the cancer cell growth was dramatically suppressed, as indicated by staining with Ki67, and inversely, TUNEL-positive apoptotic cells were growing in number at a significant level Fig. 4D). Of note, as shown in the images of COL1A1 staining, the outgrowth of the tumor matrix was also significantly downregulated by the treatment (Fig. 4D).

4. Discussion

Based on the key reports, significant S100A8/A9 expression has been detected in bladder cancer tissues [17]. In agreement with these, we provided clear images of significantly elevated S100A8/A9 staining in bladder cancer tissues compared to normal tissues (Fig. S1). However, in contrast to the results of tissue staining, we found that, in the bladder cancer cell lines used in this study, the levels of both the S100A8/A9 protein (Fig. S5A) and mRNA (Fig. S5B) were very low

or undetectable. In line with this, the elevation of S100A8/A9 in the bladder cancer tissues may derive from cancer-associated neutrophils that are highly accumulated in the cancer microenvironment. It is well known that S100A8/A9 accounts for almost half (40-45%) of the total proteins that are actively released from neutrophils in an inflammatory context [18]. Increasing evidence has shown that neutrophils actively infiltrate the bladder cancer tissues, where they gather to form neutrophil extracellular traps (NETs) [19]. We found that part of the S100A8/A9 release machinery is dependent on the formation of NETs in neutrophils (our unpublished data). In this context, it is worth noting that Sahin et al. detected much higher levels of S100A8/A9 in urine specimens from patients suffering from high-grade bladder cancers than in those from healthy donors and low-grade bladder cancer patients [7]. Conceivably, S100A8/A9 released from the infiltrated neutrophils in the cancer extracellular milieu could act on the bladder cancer cell surface, which would account for the elevated levels of the S100A8/A9 protein in some of the bladder cancer tissues of advanced grade.

Our observation of TPL2 on the TLR4 signaling pathways also merits discussion. To our surprise, our binding screening of MAPKKKs on TLR4 just beneath the plasma membrane revealed potential interactions of MAPKKKs through the TIRAP adaptor in most cases, as shown in Fig. S2B. Because we found that TPL2 was the most dominantly expressed of these MAPKKKs in the bladder cancer cell lines tested here, we kept our attention trained on TPL2 in this study context. We are of course not disregarding the significance of MAPKKKs other than TPL2, which may also have a significant role downstream of TLR4 in the other cell types in which they are themselves dominantly expressed. To the best of our knowledge, however, this is the first report to describe the presence of TPL2 beneath the TLR4-TIRAP pathway that plays a critical role in bladder cancer growth and invasion/motility. ERK is a major client kinase of TPL2, which we also confirmed in this study, so that the TPL2-ERK axis may lead to enhanced growth, migration and invasion in bladder cancer cells, since ERK is strongly associated with these cellular events [20]. Our previous efforts revealed that another S100A8/A9 receptor, MCAM, activates the TPL2-ERK pathway upon S100A8/A9 binding, which empowers breast cancer cells to activate the epithelial-mesenchymal transition (EMT) through the activation of ETV4 and subsequently ZEB1 [1]. The MCAM-TPL2-ERK pathway also functions to induce melanoma cell metastasis by co-opting the upregulation of MMP25 that is caused by the activated ETV4 [1]. Furthermore, the TPL2 activation is also regulated by RAGE, which is able to induce a high level of prostaglandin E2 (PGE2) via cyclooxygenase 2 (COX2), which in turn stimulates metastatic outgrowth of pancreatic cancers [21]. Considering that TIRAP, like TLR4, is present beneath the RAGE downstream signal [10], the previous finding of RAGE-mediated TPL2 activation [21] seems reasonable. Notably, RAGE and MCAM were also upregulated in bladder cancer cells in our present experiments (Fig. 1B). Taken together, these results lead us to speculate that the

TPL2-ERK signal exerted by TLR4 activation has an unusual role in bladder cancer growth and invasive motility through multiple downstream channels, as described above, that function in an orchestrated manner.

In line with the above results on S100A8/A9 receptor-mediated ERK activation, we also previously reported that S100A8/A9 empowers NPTNβ to lead to the dissemination of lung cancer cells via a growth factor receptor-bound protein 2 (Grb2) adaptor that firmly links to the activation of Ras and its downstream ERK [11]. Owing to the increased potential of NPTNβ—in addition to the main TLR4 and aforementioned RAGE and MCAM—in bladder cancer cells (Fig. 1A and 1B), these receptors may mutually function to activate ERK in bladder cancer cells. In line with this, we also found that there are cases where the immunohistochemistry does not match the expression patterns between S100A8/A9 and TLR4 (Fig. S1B and S1C, and Fig. 1C). In the case of TLR4-negative cancers, RAGE, MCAM or NPTNβ may function in place of TLR4 in response to S100A8/A9 in a compensatory manner.

Because the human bladder cancer cell lines used in this study have functional limitations in terms of in vivo metastasis, even when applied to a highly immunocompromised NOD/SCID mouse model, and despite our multiple attempts using different approaches, we were not able to evaluate the effect of the TLR4 inhibitor in our metastatic outgrowth model. Fortunately, however, we were able to detect a tangible anti-cancer effect of the TLR4 inhibitor in our simple tumor outgrowth model in mouse skin (Fig. 4). The tumor volumes were not substantially different between the treated and not treated groups, but the interiors of the tumors were very different from those in the non-treated controls. Specifically, we observed a significant decrease in the growth and elevation of apoptotic cells, as well as decreased formation of the cancer-associated matrix. These reduced events may provide several benefits for cancer treatment, since the dense matrices function not only as grounds for cancer cell growth and metastatic development, but also as firm barriers to drug absorption into cancer cells [22]. Therefore, the TLR4 itself and its mediated pathway identified herein may lead to the development of an effective therapeutic to prevent malignant outgrowth and possibly bladder cancer itself.

Author contributions

A.G.H.R. and N.T. established the methodology, designed and performed most of the experiments, and analyzed the data. R.K. and J.M. prepared S100A8/A9. K.Y. and H.M. prepared GST fusion proteins. S.T. and Y.I. performed the PCR experiments. T.S. and Y.G. performed the western blotting. N.L.G.Y.K., F.J., A.Y. F.K. performed the cell-based assays and animal experiments. E.K. performed the immunohistochemistry and evaluation. S.T., M.N., M.W. performed the animal experiments, and the data analysis and its evaluation and validation. M.S. performed the immunoprecipitation and western blot analysis with the assistance of A.G.H.R. and N.T. A.G.H.R. wrote the manuscript. Y.N and M.S. designed and supervised the project and wrote, reviewed and edited the manuscript.

Funding

This research was supported by a JSPS KAKENHI grant (no. 20H03516 to M.S.) and by funds to M.S. from the Nagase Science and Technology Promotion Foundation.

Acknowledgements

We gratefully acknowledge Professor Koichiro Wada (Department of Urology, Shimane University Faculty of Medicine) for technical advice on the animal experiments.

Compliance with ethical standards

Experimental protocols required for the animal studies were approved by the Animal Experiment Committee at Okayama University. The approval number is OKU-2021524.

Conflict of Interest

The authors declare that they have no conflicts of interest.

Figure legends

Fig. 1. Expression of TLR4 in bladder cancer cells and tissues, and cellular responses to S100A8/A9. A and B, Total RNAs prepared from the indicated cell lines were analyzed for the expression of the indicated S100A8/A9 receptors by RT-qPCR. The amounts of mRNA were calibrated to those of TBP mRNA (internal control) and are presented as the fold increase compared to those of the indicated controls (OUMS-24 (A) and HUC (B)). Data from A and B are means ± SD, *P<0.05, **P<0.01 and ***P<0.001 by Student's *t*-test (n = 3). C, A bladder cancer tissue array was immunohistochemically stained for TLR4. Staining results were observed macroscopically (left) and microscopically (right). Bars represent 50 μm in the magnified images (right). D and E, J82 cells were treated with either LPS (100 ng/ml) or S100A8/A9 (1 μg/ml) for one day, or left untreated. Cell growth (D) and migration (E) of the stimulated cells were evaluated by MTS and Boyden chamber assays, respectively. In the Boyden chamber procedure, cells were placed in the top chamber and LPS (100 ng/ml) or purified recombinant S100A8/A9 (1 μg/ml) was added to the bottom well. Data from D and E are means ± SD, *P<0.05, **P<0.01 and ***P<0.001 by Student's *t*-test (n = 3). F, Phosphorylation status of ERK was examined by WB of the J82 cells stimulated with either LPS (100 ng/ml) or S100A8/A9 (1 μg/ml) for the indicated times. G, Dose-dependent alteration of the ERK phosphorylation was also evaluated for S100A8/A9 at 30 min after the stimulations. H, Phosphorylation conditions were evaluated for the indicated effector kinases other than ERK in the J82 cells stimulated with LPS (100 ng/ml) or S100A8/A9 (1 μg/ml) for 30 min. β-actin detection and Coomassie brilliant blue (CBB) staining were used as loading controls (F, G and H). The WB were repeated three times for each set of samples (F, G and H).

Fig. 2. TPL2 on the TLR4-downstream plays a critical role in the growth, migration and invasion of bladder cancer cells. A, RT-qPCR analysis was carried out in the indicated cells for the candidate genes. The relative expression level in each sample is shown after calibration with the TBP value and is presented as the fold increase compared to those of the indicated controls (OUMS-24 for TAK1, DLK, TPL2 and ARAF; HEK293T for MOS). Data are means ± SD, *P<0.05, **P<0.01 and ***P<0.001 by Student's *t*-test (n = 3). ND: Not detected. B, Overview of the predicted MAPK cascade that is activated in the presence of TLR4 upon the binding with the ligands. C, Standard growth (left), migration (middle) and invasion (right) were evaluated in J82 cells with or without overexpression of TPL2 KD by the MTS assay and Boyden chamber-based migration and invasion assays, respectively. In these experimental contexts, cells were treated with LPS (100 ng/ml) for one day. D and E, Experiments similar to those shown in panel C were also conducted for J82 cells that were treated with either LPS (100 ng/ml, one day) or S100A8/A9 (1 μg/ml, one day) in the presence or absence of TPL2 inhibitor (1 μM) (D) and

TIRAP inhibitory peptide (40 μM) (E). The data in panels C, D and E are means ± SD, *P<0.05, **P<0.01 and ***P<0.001 by Student's *t*-test (n = 3).

Fig. 3. Significant role of TIRAP in the activation of TPL2. A, The pulled-down TPL2 WT was mixed with the prepared recombinant proteins according to the indicated formula and the mixed solutions were then incubated for 10 min or an extended 60 min in the presence or absence of the TPL2 inhibitor. The reactants were then subjected to WB with the indicated antibodies. B, A similar experiment as performed in A was also implemented by using the inactive form of TPL2 (TPL2 KD) in comparison to the wild-type counterpart (TPL2 WT). C, The dose-dependent effect of GST-TIRAP on TPL2 activation was further evaluated using experiments similar to those shown in panels A and B. These experiments were repeated an additional two times for each set of samples (A, B and C). D, J82 cells were treated with either LPS (100 ng/ml) or S100A8/A9 (1 μg/ml) for 30 min in the presence or absence of a TPL2 inhibitor (1 μM). The treated cells were lysed and subjected to IP using the indicated biotinylated (bio) antibodies, and the precipitates were further subjected to WB with the indicated antibodies. A series of each experiment was repeated at least three times.

Fig. 4. Critical role of TLR4 in bladder cancer survival in vivo. A, B and C**,** The sizes of J82 cell-derived tumors were monitored on the indicated days. 200 μl of TLR4 inhibitor (Resatorvid 300 μg/ml in DMSO) was intraperitoneally administered (in a volume corresponding to approximately 30 μg/ml (80 nM) in vitro) starting at day 0 (the tumor volumes reached about 150 mm^3) and then every other day (A). On day 64, the resected tumors were all weighed (B) and imaged (C). Data from A and B are means ± SD, *P<0.05 and **P<0.01 by Student's *t*-test (n = 4). D, Tissue sections were prepared from the resected tumors and stained with either immunofluorescence (left images) or hematoxylin and eosin (H&E) (right images) to study their intratumor conditions. The appearance of proliferating cells and apoptotic cells was evaluated by the staining procedures using anti-Ki67 antibody and the TUNEL method, respectively. The status of cancer-associated matrix formation was also evaluated by staining with anti-COL1A1 antibody. The bars in the images represent 50 μm. The stained images at left were all quantified as shown at right. Data are means ± SD. *p<0.05 and ***p<0.001 by Student's *t*-test (n = 3).

References

1. N. Tomonobu, R. Kinoshita, M. Sakaguchi, S100 Soil sensor receptors and molecular targeting therapy against them in cancer metastasis, *Transl. Oncol.* 13 (2020) 100753.
2. S. Hiratsuka, A. Watanabe, H Aburatani, Y. Maru, Tumour-mediated upregulation of chemoattractants and recruitment of myeloid cells predetermines lung metastasis, *Nat. Cell Biol.* 8 (2006) 1369-1375.
3. A. Saha, Y.C. Lee, Z. Zhang, G. Chandra, S.B. Su, A.B. Mukherjee, Lack of an endogenous anti-inflammatory protein in mice enhances colonization of B16F10 melanoma cells in the lungs, *J. Biol. Chem.* 285 (2010) 10822-10831.
4. A.T. Lenis, P.M. Lec, K. Chamie, M.D. Mshs, Bladder cancer: a review, *J.A.M.A.* 324 (2020) 1980-1991.
5. M.S. Zaghloul, T.M. Zaghloul, M.K. Bishr, B.C. Baumann, Urinary schistosomiasis and the associated bladder cancer: update, *J. Egypt. Natl. Canc. Inst.* 32 (2020) 44.
6. S. Letasiova, A. Medve'ova, A. Sovcikova, et al, Bladder cancer, a review of the environmental risk factors, *Environ. Health* 11 (2012) Suppl 1:S11.
7. Y. Sahin, U. Yucetas, H.A. Ates, et al, Improving the diagnosis of high grade and stage bladder cancer by detecting increased urinary calprotectin expression in tumor tissue and tumor-associated inflammatory response, *Investig. Clin. Urol.* 60 (2019) 343-350.
8. M. Sakaguchi, M. Watanabe, R. Kinoshita, et al, Dramatic increase in expression of a transgene by insertion of promoters downstream of the cargo gene, *Mol. Biotechnol.* 56 (2014) 621-630.
9. J. Futami, Y. Atago, A. Azuma, et al, An efficient method for the preparation of preferentially heterodimerized recombinant S100A8/A9 coexpressed in Escherichia coli, *Biochem. Biophys. Rep.* 94 (2016) 94-100.
10. M. Sakaguchi, H. Murata, K. Yamamoto, et al, TIRAP, an adaptor protein for TLR2/4, transduces a signal from RAGE phosphorylated upon ligand binding, *PLoS One* 6 (2011) e23132.
11. M. Sakaguchi, M. Yamamoto, M. Miyai, et al, Identification of an S100A8 receptor neuroplastin-β and its heterodimer formation with EMMPRIN, *J. Invest. Dermatol.* 136 (2016) 2240-2250.
12. M. Sakaguchi, T. Kondo, H. Pu, M. Namba, Transferrin synthesized in cultured human fibroblasts is associated with Dublin's and has iron binding capacity, *Cell Struct. Funct.* 24 (1999) 5-9.
13. H. Takamatsu, KI. Yamamoto, N. Tomonobu, et al, Extracellular S100A11 Plays a Critical Role in Spread of the Fibroblast Population in Pancreatic Cancers, *Oncol. Res.* 27 (2019) 713-727.

14. F. Hua, H. Tang, J. Wang, et al, TAK-242, an antagonist for Toll-like receptor 4, protects against acute cerebral ischemia/reperfusion injury in mice, *J. Cereb. Blood Flow Metab.* 35 (2015) 536-542.
15. S. Akira, S. Uematsu, O. Takeuchi, Pathogen recognition and innate immunity, *Cell* 124 (2006) 783-801.
16. M. Karlou, A.A. Saetta, O. Korkolopoulou, et al, Activation of extracellular regulated kinases (ERK1/2) predicts poor prognosis in urothelial bladder carcinoma and is not associated with B-Raf gene mutations, *Pathology* 41 (2009) 327-334.
17. S. Minami, Y. Sato, T. Matsumoto, et al, Proteomic study of sera from patients with bladder cancer: usefulness of S100A8 and S100A9 proteins, *Cancer Genomics Proteomics* 7 (2010) 181-189.
18. S. Wang, R. Song, Z. Wang, Z. Jing, S. Wang, J. Ma, S100A8/A9 in Inflammation, *Front. Immunol.* 9 (2018) 1298.
19. S. Shinde-Jadhav, J.J. Mansure, R.F. Rayes, et al, Role of neutrophil extracellular traps in radiation resistance of invasive bladder cancer, *Nat. Commun.* 12 (2021) 2776.
20. M. Kohno, J. Pouyssegur, Targeting the ERK signaling pathway in cancer therapy, *Ann. Med.* 38 (2006) 200-211.
21. Y. Mitsui, N. Tomonobu, M. Watanabe, et al, Upregulation of mobility in pancreatic cancer cells by secreted S100A11 through activation of surrounding fibroblasts, *Oncol. Res.* 27 (2019) 945-956.
22. K.C. Valkenburg, A.E. de Groot, K.J. Pienta, Targeting the tumour stroma to improve cancer therapy, *Nat. Rev. Clin. Oncol.* 15 (2018) 366-381.

Rodrigo and Tomonobu et al.

Figures

Fig.1

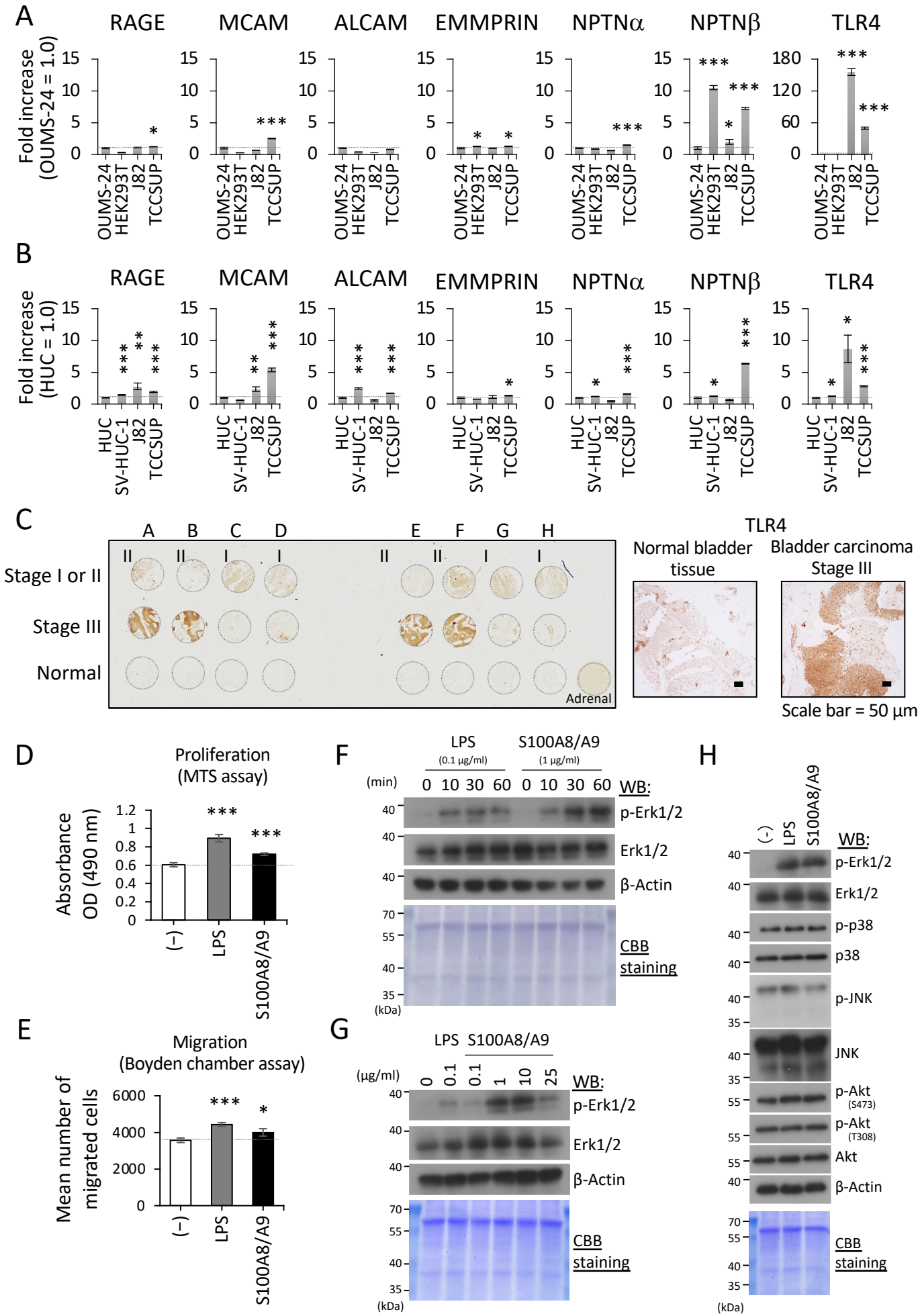
A
RAGE
MCAM
ALCAM
EMMPRIN
NPTNα
NPTNβ
TLR4
Fold increase (OUMS-24 = 1.0)
OUMS-24
HEK293T
J82
TCCSUP
B
Fold increase (HUC = 1.0)
HUC
SV-HUC-1
C
Stage I or II
Stage III
Normal
Adrenal
TLR4
Normal bladder tissue
Bladder carcinoma Stage III
Scale bar = 50 μm
D
Proliferation (MTS assay)
Absorbance OD (490 nm)
(–)
LPS
S100A8/A9
E
Migration (Boyden chamber assay)
Mean number of migrated cells
F
LPS (0.1 μg/ml)
S100A8/A9 (1 μg/ml)
(min)
WB:
p-Erk1/2
Erk1/2
β-Actin
CBB staining
(kDa)
G
(μg/ml)
H
p-p38
p38
p-JNK
JNK
p-Akt (S473)
p-Akt (T308)
Akt

Fig. 2

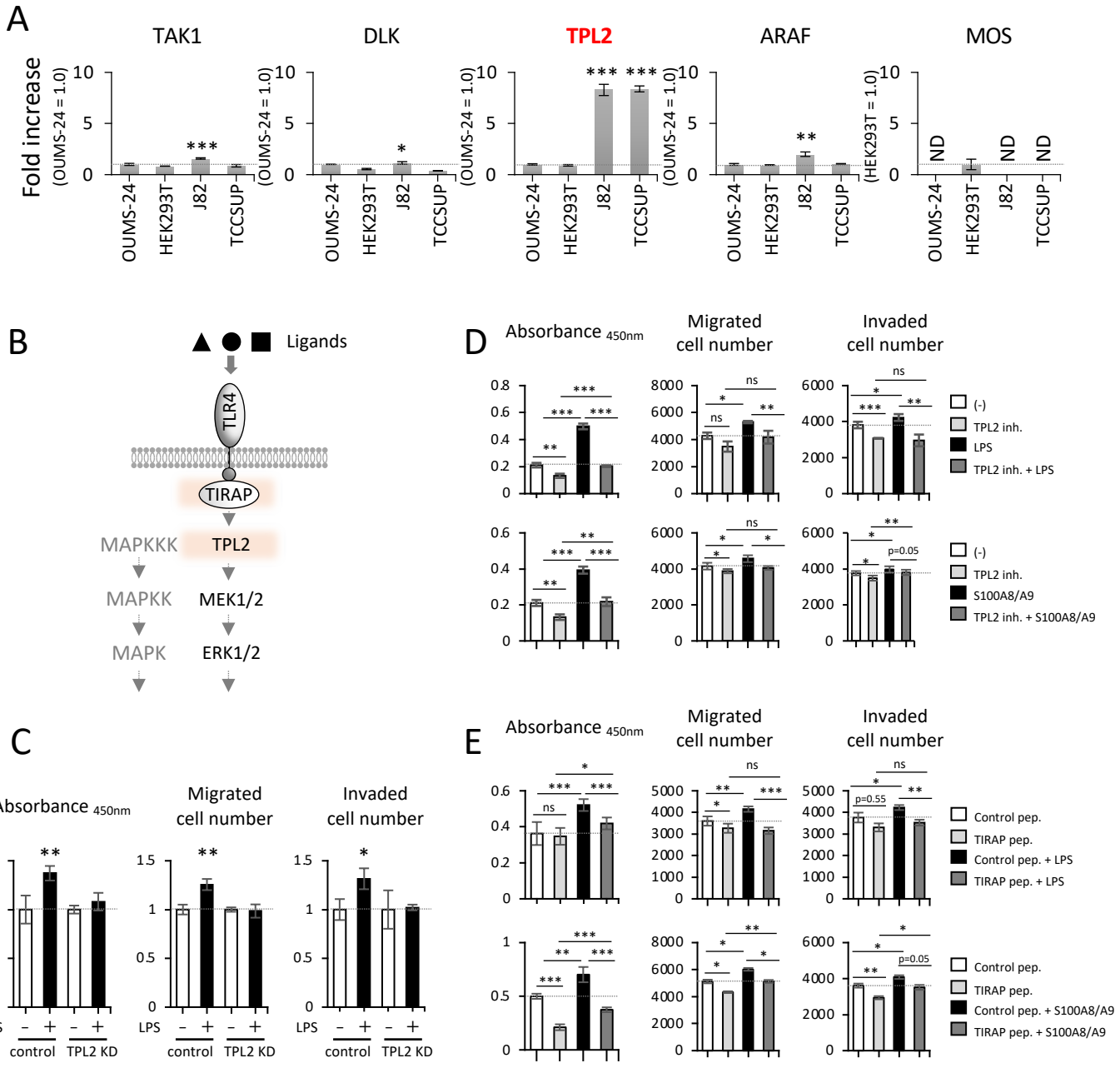
A
TAK1
DLK
TPL2
ARAF
MOS
Fold increase
(OUMS-24 = 1.0)
(HEK293T = 1.0)
OUMS-24
HEK293T
J82
TCCSUP
ND
B
Ligands
TLR4
TIRAP
MAPKKK
TPL2
MAPKK
MEK1/2
MAPK
ERK1/2
C
Absorbance 450nm
Migrated cell number
Invaded cell number
LPS
control
TPL2 KD
D
Absorbance 450nm
Migrated cell number
Invaded cell number
(-)
TPL2 inh.
LPS
TPL2 inh. + LPS
S100A8/A9
TPL2 inh. + S100A8/A9
p=0.05
E
Absorbance 450nm
Migrated cell number
Invaded cell number
Control pep.
TIRAP pep.
Control pep. + LPS
TIRAP pep. + LPS
Control pep. + S100A8/A9
TIRAP pep. + S100A8/A9
p=0.55
p=0.05

Fig. 3

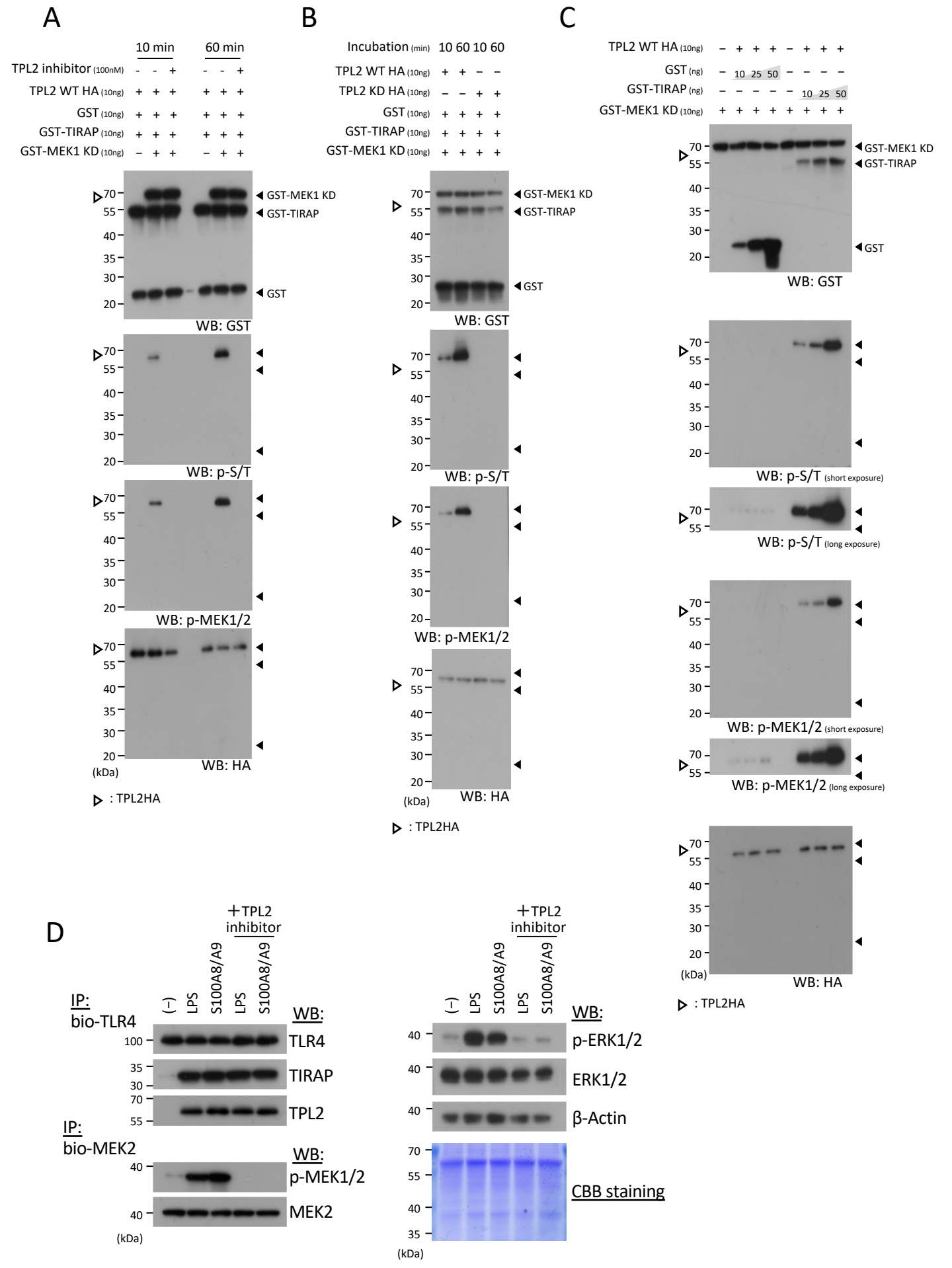
A
10 min
60 min
TPL2 inhibitor (100nM)
TPL2 WT HA (10ng)
GST (10ng)
GST-TIRAP (10ng)
GST-MEK1 KD (10ng)
GST-MEK1 KD
GST-TIRAP
GST
WB: GST
WB: p-S/T
WB: p-MEK1/2
WB: HA
(kDa)
: TPL2HA
B
Incubation (min) 10 60 10 60
TPL2 WT HA (10ng)
TPL2 KD HA (10ng)
GST (10ng)
GST-TIRAP (10ng)
GST-MEK1 KD (10ng)
C
TPL2 WT HA (10ng)
GST (ng)
GST-TIRAP (ng)
GST-MEK1 KD (10ng)
WB: p-S/T (short exposure)
WB: p-S/T (long exposure)
WB: p-MEK1/2 (short exposure)
WB: p-MEK1/2 (long exposure)
D
+TPL2 inhibitor
(–)
LPS
S100A8/A9
IP: bio-TLR4
WB:
TLR4
TIRAP
TPL2
IP: bio-MEK2
p-MEK1/2
MEK2
p-ERK1/2
ERK1/2
β-Actin
CBB staining

Fig. 4

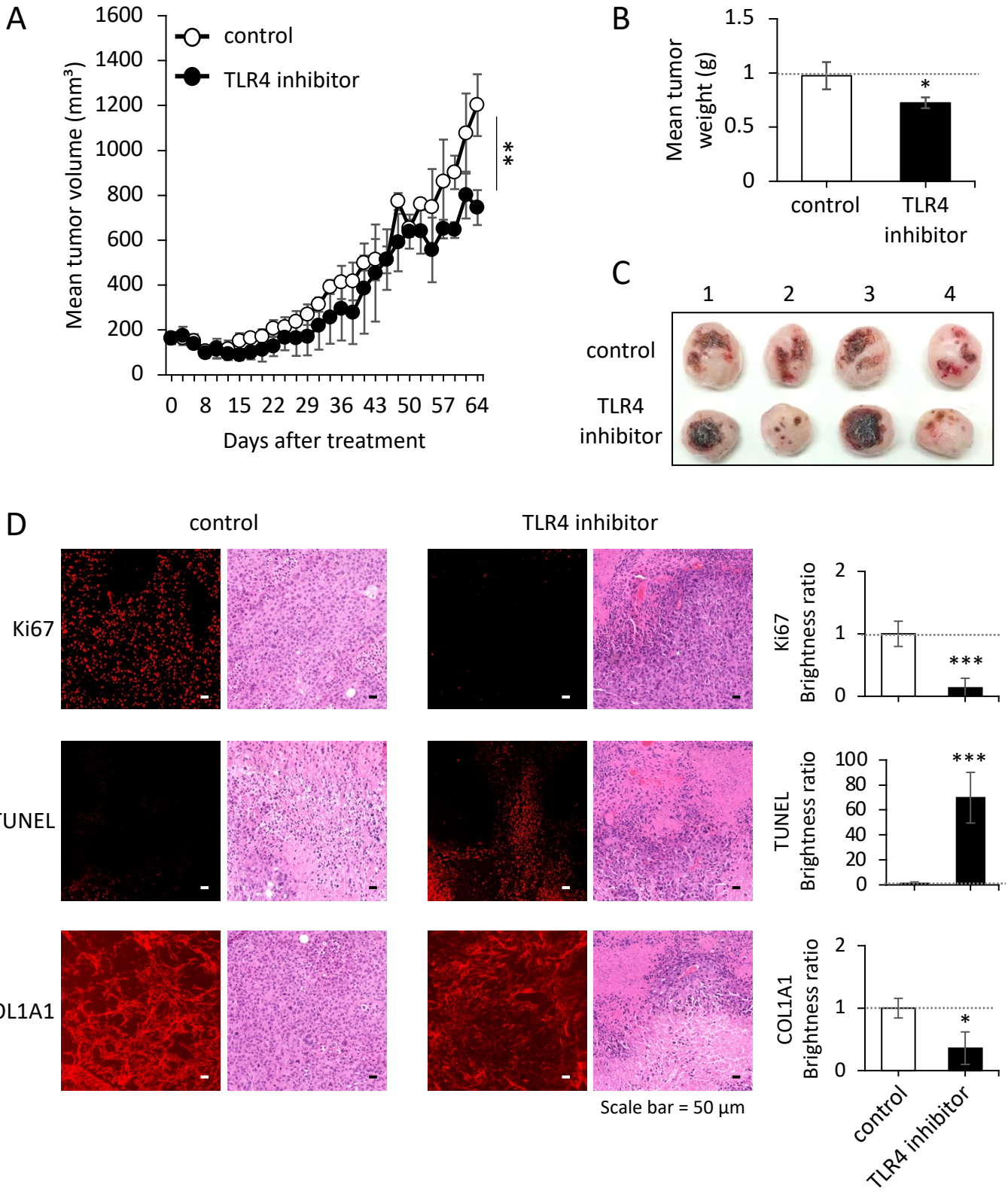
A
Mean tumor volume (mm³)
1600
1400
1200
1000
800
600
400
200
0
control
TLR4 inhibitor
**
0 8 15 22 29 36 43 50 57 64
Days after treatment
B
Mean tumor weight (g)
1.5
1
0.5
0
*
control
TLR4 inhibitor
C
1 2 3 4
control
TLR4 inhibitor
D
control
TLR4 inhibitor
Ki67
TUNEL
COL1A1
Ki67 Brightness ratio
***
TUNEL Brightness ratio
***
COL1A1 Brightness ratio
*
control
TLR4 inhibitor
Scale bar = 50 µm

Supplementary Information

Supplementary Figure (Fig. S) Legends

Fig. S1. Immunostaining of S100A8/A9 in bladder cancer tissues. A, H&E staining. Staining results were observed macroscopically (top) and microscopically (bottom). B and C, Staining results were observed macroscopically (left) and microscopically (right). S100A8 and S100A9 were detected in the brown-colored cancer lesions. Bars represent 50 μm in the magnified images.

Fig. S2. Screening of MAPKKK(s) that presents on the TLR4-downstream MAPK cascade. A, Schematic diagram of the MAPK cascade B, HEK293T cells were co-transfected with Flag-tagged TLR4 and Myc-tagged upstream kinases: NAK (NF-κB-Activating Kinase: gene name, *TBK1*), NIK (NF-κB-Inducing Kinase: gene name, *MAP3K14*), TAK1 (TGF-β-Activated Kinase 1: gene name, *MAP3K7*), DLK (Dual Leucine Zipper-Bearing Kinase: gene name, *MAP3K12*), TPL2 (Tumor Progression Locus 2: gene name, *MAP3K8*), ASK1 (Apoptosis Signal-Regulating Kinase 1: gene name, *MAP3K5*), SPRK (Src-Homology 3 Domain-Containing Proline-Rich Kinase: gene name, *MAP3K11*), MLK1 (Mixed Lineage Kinase 1: gene name, *MAP3K9*), MEKK3 (MAPK/ERK Kinase 3: gene name, *MAP3K3*), LZK (Leucine Zipper-Bearing Kinase: gene name, *MAP3K13*), MLK4 (Mixed Lineage Kinase 4: gene name, *MAP3K21*), ARAF (A-Raf Proto-Oncogene, Serine/Threonine Kinase: gene name, *ARAF*), BRAF (B-Raf Proto-Oncogene, Serine/Threonine Kinase: gene name, *BRAF*), CRAF (C-Raf Proto-Oncogene, Serine/Threonine Kinase: *RAF1*) and MOS (MOS Proto-Oncogene, Serine/Threonine Kinase: *MOS*). After IP of the expressed TLR4 with Flag antibody-conjugated beads, interacting kinases were detected by the Myc antibody (left). An experiment similar to that shown in the left panel was performed, except that the HA-tagged TLR4 adaptors (TIRAP, MyD88 or TRAM) were used for co-transfection with the selected kinases and HA antibody-conjugated beads were used for IP of the expressed foreign adaptors (right). The interacting candidates are highlighted in red (left and right). The data were confirmed by two independent experiments.

Fig. S3. Preparation of recombinant proteins for in vitro kinase reaction. A, Prepared recombinant proteins (GST, GST-MEK1 KD and GST-TIRAP) from the E. coli expression system were checked for their purity. B and C, Pulled-down TPL2-HA (WT and KD) were also checked for their actual inclusions in the precipitates by silver staining (B) and WB with anti-HA antibody (C). As for the confirmation experiments in B and C, the degree of the intrinsic TIRAP inclusions for the immunoprecipitates was also checked by WB using the specific antibody, since the

presence of cellular TIRAP may affect the TPL2 activation in a cell-free system dependent on its contamination degree (D). Confirmation of the material preparations through the experiments (from A through D) were repeated an additional two times.

Fig. S4. Critical role of TPL2 in the activation of ERK through TIRAP binding upon the ligand stimulations of bladder cancer cells. TCCSUP cells were treated with either LPS (100 ng/ml) or S100A8/A9 (1 μg/ml) for 30 min in the presence or absence of a TPL2 inhibitor (1 μM). The treated cells were lysed and subjected to IP using the indicated biotinylated antibodies (bio-TLR4 and bio-MEK2), and the precipitates were further subjected to WB with the indicated antibodies (TLR4, TIRAP, TPL2, P-MEK1/2 and MEK2). The experiments (IP-WB and WB) were repeated at least three times.

Fig. S5. Measurement of S100A8/A9 levels in human cells. A, S100A8/A9 levels in the cultured cells were measured and quantified by a conventional ELISA. Cells and their conditioned media indicated beneath the bar graphs were collected. The collected cell pellets were lysed with M-PER solution (Thermo Fisher Scientific). The collected cell lysates and their corresponding culture media were then subjected to the sandwich ELISA method using our developed S100A8/A9 antibodies (clone #260 was set on the plate and clone #45 conjugated with biotin was used for detection) to monitor the levels of intrinsic S100A8/A9 protein in the specimens. A431 cells were used as a positive control for S100A8/A9 detection; these cells show active production of S100A8/A9 and release of the protein to the extracellular space. B, The indicated leukocytes were collected from the blood specimen of a healthy donor. In brief, leukocytes were separated into two fractions, a mononuclear cell fraction and a polymorphonuclear fraction, by using polymorphprep (Abbot Diagnostics Technologies AS, Oslo, Norway). The monocytes, NK cells, CD4+T cells, and Treg cells were then isolated from the mononuclear cell fraction using CD14 MicroBeads, human (Miltenyi Biotec, Bergisch Gladbach, Germany), an NK Cell Isolation Kit, human (Miltenyi Biotec), CD4 MicroBeads, human (Miltenyi Biotec), and a CD4+CD25+ Regulatory T Cell Isolation Kit, human (Miltenyi Biotec), respectively. On the other hand, neutrophils were isolated from the separated polymorphonuclear fraction using CD16 MicroBeads, human (Miltenyi Biotec) (CD16 positive: neutrophils). Total RNAs prepared from the indicated cells were analyzed for the expression of the S100A8 and S100A9 by RT-qPCR. The amounts of mRNA were calibrated to those of TBP mRNA (internal control) and are presented as the fold increase relative to those of the indicated controls (NK cells (left) and MMAc (right)). Data are means ± SD, *P<0.05, **P<0.01 and ***P<0.001 by Student's *t*-test (n = 3). ND: Not detected.

Supplementary Tables (Table S)

Table S1. Cell lines

Cells		Medium	Source
OUMS-24*	Normal human fibroblasts	DMEM/F12 + 10% FBS (Thermo Fisher Scientific, Waltham, MA)	Dr. Masayoshi Namba
HEK293T	Non-cancerous human embryonic kidney epithelial cell line with stable expression of the simian virus 40 (SV40) large T antigen	DMEM/F12 + 10% FBS (Thermo Fisher Scientific)	RIKEN BioResource Center (Tsukuba, Japan)
HUC	Normal human uroepithelial cells	Urothelial Cell Medium (ScienCell Research Laboratories)	ScienCell Research Laboratories (Carlsbad, CA, USA)
SV-HUC-1	SV40-transformed immortal HUC cells	DMEM/F12 + 10% FBS (Thermo Fisher Scientific)	ATCC (Rockville, MD)
J82	Human urinary bladder transitional carcinoma cell lines	DMEM/F12 + 10% FBS (Thermo Fisher Scientific)	ATCC
TCCSUP	Human urinary bladder transitional carcinoma cell lines	DMEM/F12 + 10% FBS (Thermo Fisher Scientific)	ATCC

* R. Ohashi, M. Miyazaki, K. Fushimi, et al, Enhanced activity of cyclin A-associated kinase in immortalized human fibroblasts, Int. J. Cancer 82 (1999) 754-758.

Table S2. Primary antibodies for IHC

Antibody	Commercial source
Rabbit anti-human S100A8 antibody	Santa Cruz Biotechnology, Dallas, TX
Rabbit anti-human S100A9 antibody	Santa Cruz Biotechnology
Mouse anti-human TLR4 antibody	Proteintech, Rosemon, IL
Rabbit anti-human Ki-67 (Ki67)	NeoMarkers, Fremont, CA
Rabbit anti-human collagen type 1 alpha 1 chain (COL1A1)	Cell Signaling Technology, Danvers, MA

Table S3. Primer sequences for RT-qPCR

Target	Forward (5' to 3')	Reverse (5' to 3')
TBP	GAACATCATGGATCAGAACAACA	ATAGGGATTCCGGGAGT
RAGE (AGER)	GGCAGACAGAGCCAGGAC	AGCACCCAGGCTCCAACT
MCAM	CACCGTCCCTGTTTTCTACC	TCCCCTTCCTTCAGCATTC
NPTNα	TCTCGCTGTTGCTGGTCTC	CAGGGCTGTCTCGAATAATGA
NPTNβ	AGGCAAAACCCCTCCATAAC	CAGGGCTGTCTCGAATAATGA
ALCAM	GGCAGTGGAAGCGTCATAA	CATTCTCTTCAGGGGAAATGA
EMMPRIN (BSG)	GAATGACAGCGCCACAGAG	TACTCTCCCCACTGGTCGTC
TLR4	GAACACCAGAGTTTCCTGCAA	TGCCCTGCTTATCTGAAGGT
TAK1 (MAP3K7)	AACTCCATCCCAATGGCTTA	CAATGCTGTTCAAACACTGC
DLK (MAP3K12)	CCATTCCACACCAGGAACTTC	GCATCAACGCTGTTGGAGTTG
TPL2 (MAP3K8)	AGGACCTCCGAGGAACAGA	CCGTCTGCATGTGGATGA
ARAF	TGGTCTACCGACTCATCAAGG	CAAGGACCTCGACAATGAGC
MOS	TTGTGCACTTGGACCTGAAG	AGCACAGCAGATCTTCCAAC

Table S4. Primary antibodies for WB

Antibody	Commercial source
Mouse anti-Myc tag antibody	Cell Signaling Technology
Mouse anti-human TLR4	Santa Cruz Biotechnology
Rabbit anti-human TIRAP	abcam, Cambridge, UK
Rabbit anti-human TPL2	Cell Signaling Technology
Mouse anti-human phospho-MEK1/2 (Ser218/222)	BD Biosciences, Franklin Lakes, NJ
Rabbit anti-human MEK2	Cell Signaling Technology
Rabbit anti-human phospho-p44/42 MAPK (Erk1/2) (Thr202/Tyr204)	Cell Signaling Technology
Rabbit anti-human p44/42 MAPK (Erk1/2)	Cell Signaling Technology
Rabbit anti-human phospho-p38 MAPK (Thr180/Tyr182)	Cell Signaling Technology
Rabbit anti-human p38 MAPK	Cell Signaling Technology
Rabbit anti-human phospho-SAPK/JNK (Thr183/Tyr185)	Cell Signaling Technology
Rabbit anti-human SAPK/JNK	Cell Signaling Technology
Rabbit anti-human phospho-Akt (Ser473)	Cell Signaling Technology
Rabbit anti-human phospho-Akt (Thr308)	Cell Signaling Technology
Rabbit anti-human Akt	Cell Signaling Technology
Mouse anti-β-actin	Sigma-Aldrich, St. Louis, MO

Rodrigo and Tomonobu et al.

Supplementary Figures (Fig. S)

Fig. S1

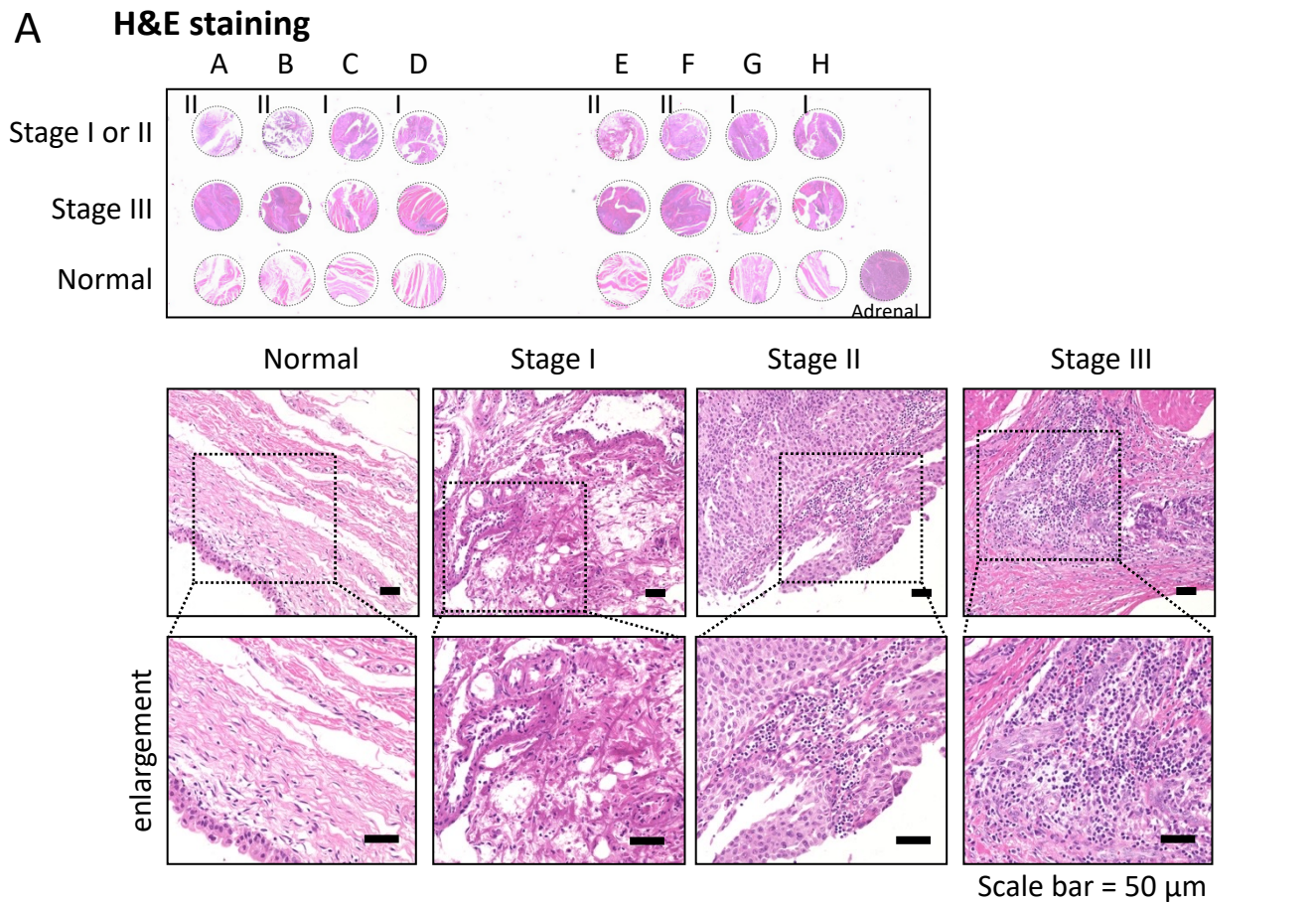

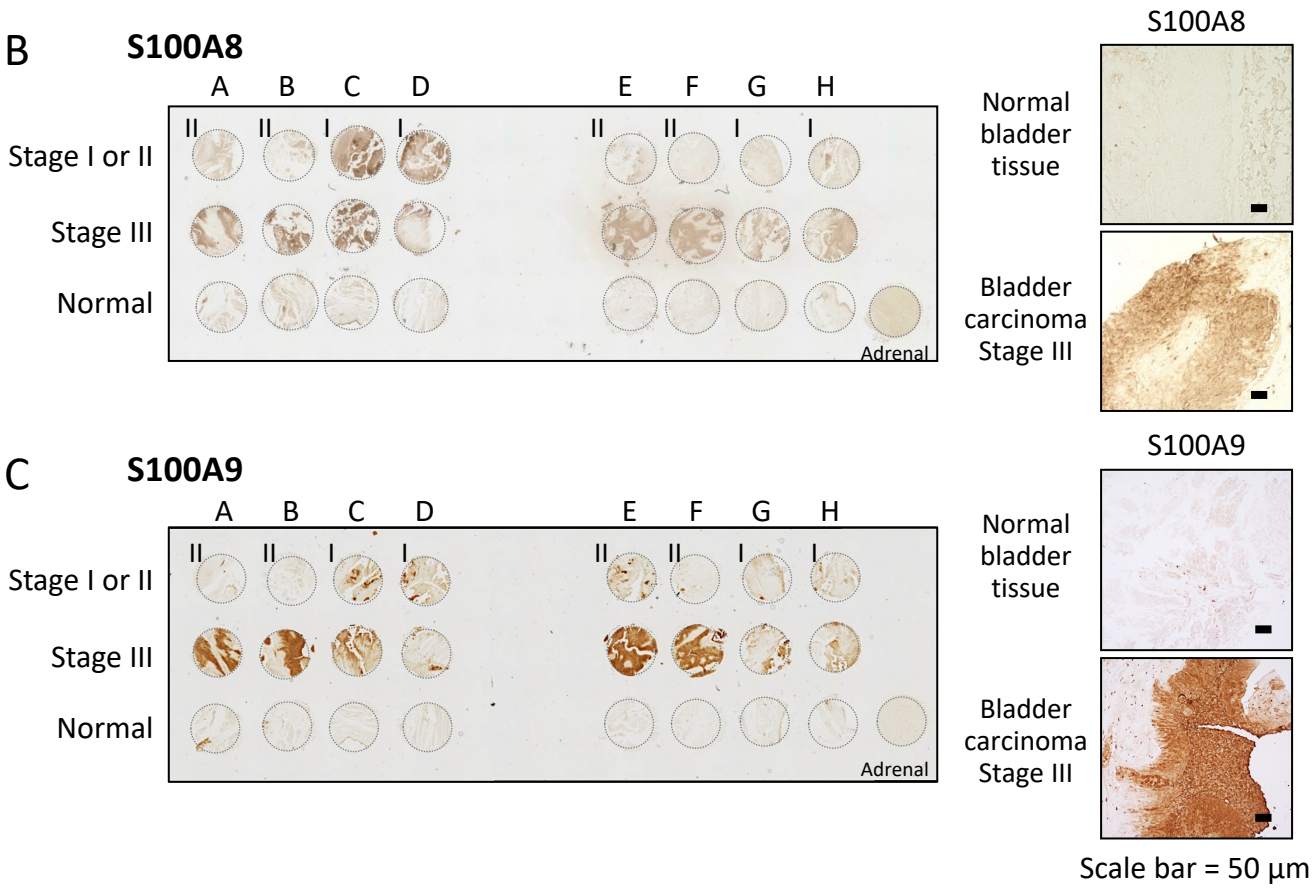

Fig. S1. Immunostaining of S100A8/A9 in bladder cancer tissues. A, H&E staining. Staining results were observed macroscopically (top) and microscopically (bottom). B and C, Staining results were observed macroscopically (left) and microscopically (right). S100A8 and S100A9 were detected in the brown-colored cancer lesions. Bars represent 50 μm in the magnified images.

Fig. S2

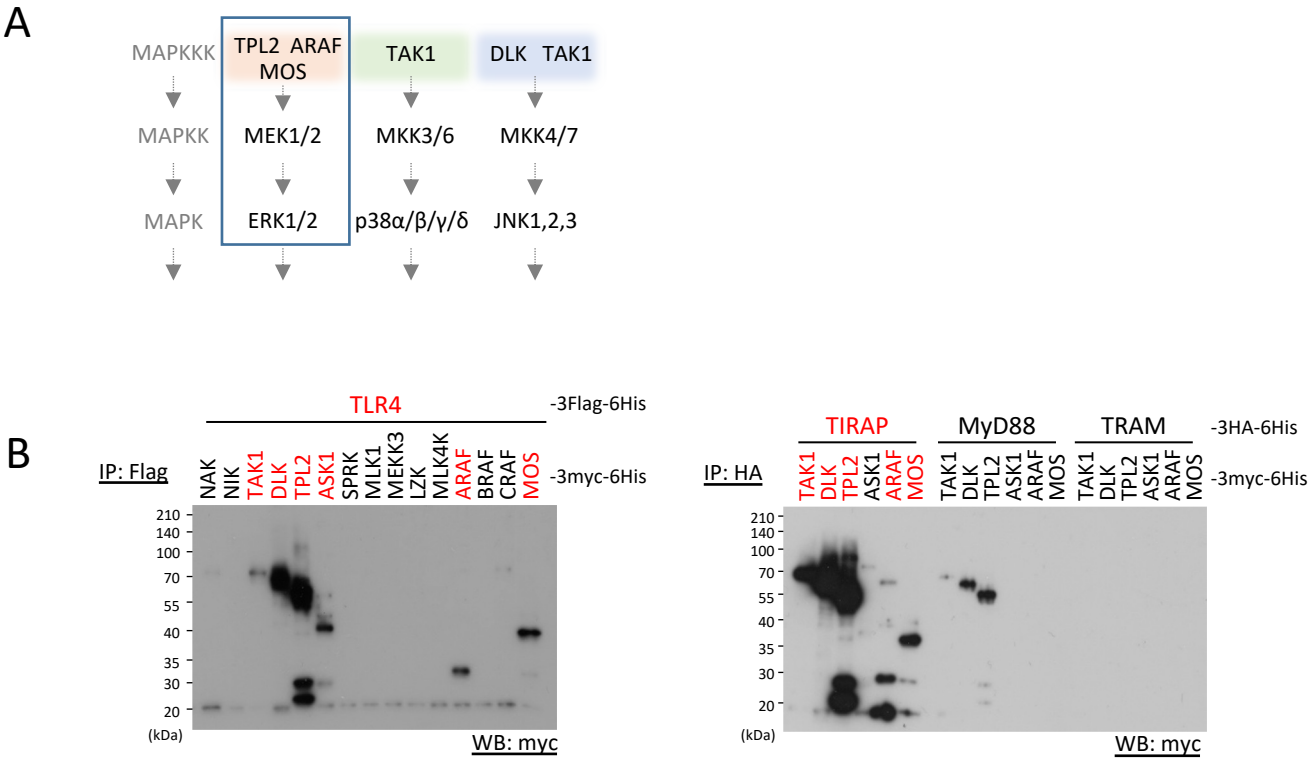

Fig. S2. Screening of MAPKKK(s) that presents on the TLR4-downstream MAPK cascade. A, Schematic diagram of the MAPK cascade B, HEK293T cells were co-transfected with Flag-tagged TLR4 and Myc-tagged upstream kinases: NAK (NF-κB-Activating Kinase: gene name, *TBK1*), NIK (NF-κB-Inducing Kinase: gene name, *MAP3K14*), TAK1 (TGF-β-Activated Kinase 1: gene name, *MAP3K7*), DLK (Dual Leucine Zipper-Bearing Kinase: gene name, *MAP3K12*), TPL2 (Tumor Progression Locus 2: gene name, *MAP3K8*), ASK1 (Apoptosis Signal-Regulating Kinase 1: gene name, *MAP3K5*), SPRK (Src-Homology 3 Domain-Containing Proline-Rich Kinase: gene name, *MAP3K11*), MLK1 (Mixed Lineage Kinase 1: gene name, *MAP3K9*), MEKK3 (MAPK/ERK Kinase 3: gene name, *MAP3K3*), LZK (Leucine Zipper-Bearing Kinase: gene name, *MAP3K13*), MLK4 (Mixed Lineage Kinase 4: gene name, *MAP3K21*), ARAF (A-Raf Proto-Oncogene, Serine/Threonine Kinase: gene name, *ARAF*), BRAF (B-Raf Proto-Oncogene, Serine/Threonine Kinase: gene name, *BRAF*), CRAF (C-Raf Proto-Oncogene, Serine/Threonine Kinase: *RAF1*) and MOS (MOS Proto-Oncogene, Serine/Threonine Kinase: *MOS*). After IP of the expressed TLR4 with Flag antibody-conjugated beads, interacting kinases were detected by the Myc antibody (left). An experiment similar to that shown in the left panel was performed, except that the HA-tagged TLR4 adaptors (TIRAP, MyD88 or TRAM) were used for co-transfection with the selected kinases and HA antibody-conjugated beads were used for IP of the expressed foreign adaptors (right). The interacting candidates are highlighted in red (left and right). The data were confirmed by two independent experiments.

Fig. S3

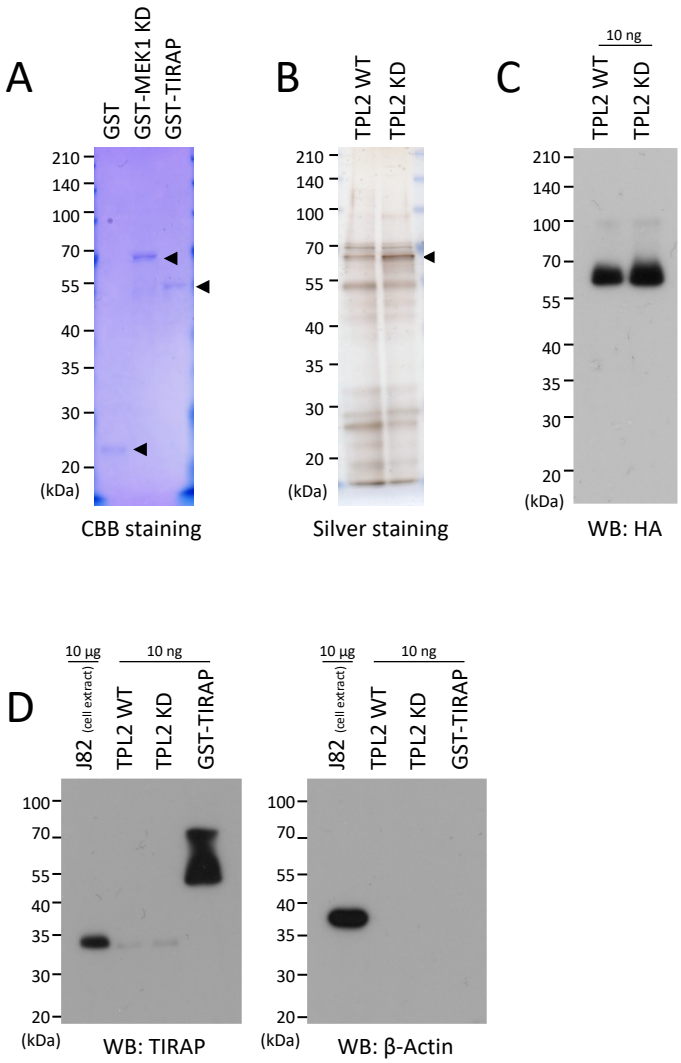

Fig. S3. Preparation of recombinant proteins for in vitro kinase reaction. A, Prepared recombinant proteins (GST, GST-MEK1 KD and GST-TIRAP) from the E. coli expression system were checked for their purity. B and C, Pulled-down TPL2-HA (WT and KD) were also checked for their actual inclusions in the precipitates by silver staining (B) and WB with anti-HA antibody (C). As for the confirmation experiments in B and C, the degree of the intrinsic TIRAP inclusions for the immunoprecipitates was also checked by WB using the specific antibody, since the presence of cellular TIRAP may affect the TPL2 activation in a cell-free system dependent on its contamination degree (D). Confirmation of the material preparations through the experiments (from A through D) were repeated an additional two times.

Fig. S4

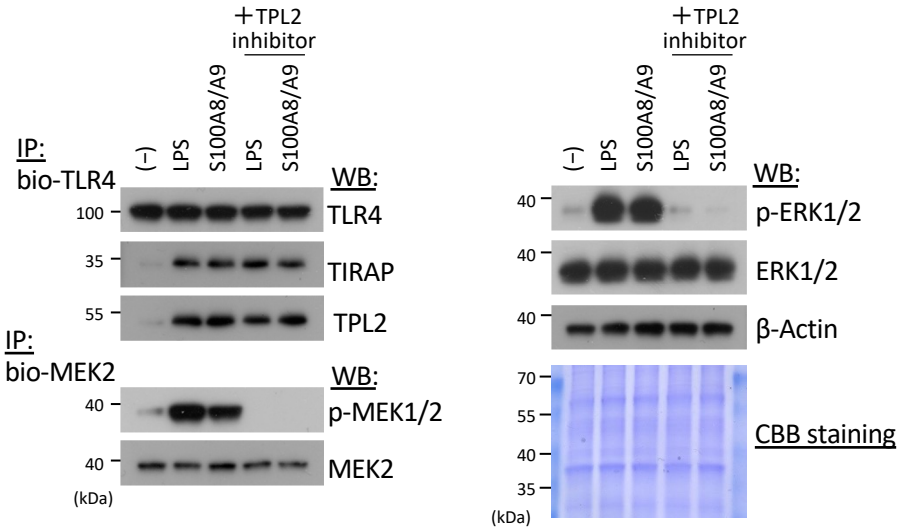

Fig. S4. Critical role of TPL2 in the activation of ERK through TIRAP binding upon the ligand stimulations of bladder cancer cells. TCCSUP cells were treated with either LPS (100 ng/ml) or S100A8/A9 (1 μg/ml) for 30 min in the presence or absence of a TPL2 inhibitor (1 μM). The treated cells were lysed and subjected to IP using the indicated biotinylated antibodies (bio-TLR4 and bio-MEK2), and the precipitates were further subjected to WB with the indicated antibodies (TLR4, TIRAP, TPL2, P-MEK1/2 and MEK2). The experiments (IP-WB and WB) were repeated at least three times.

Fig. S5

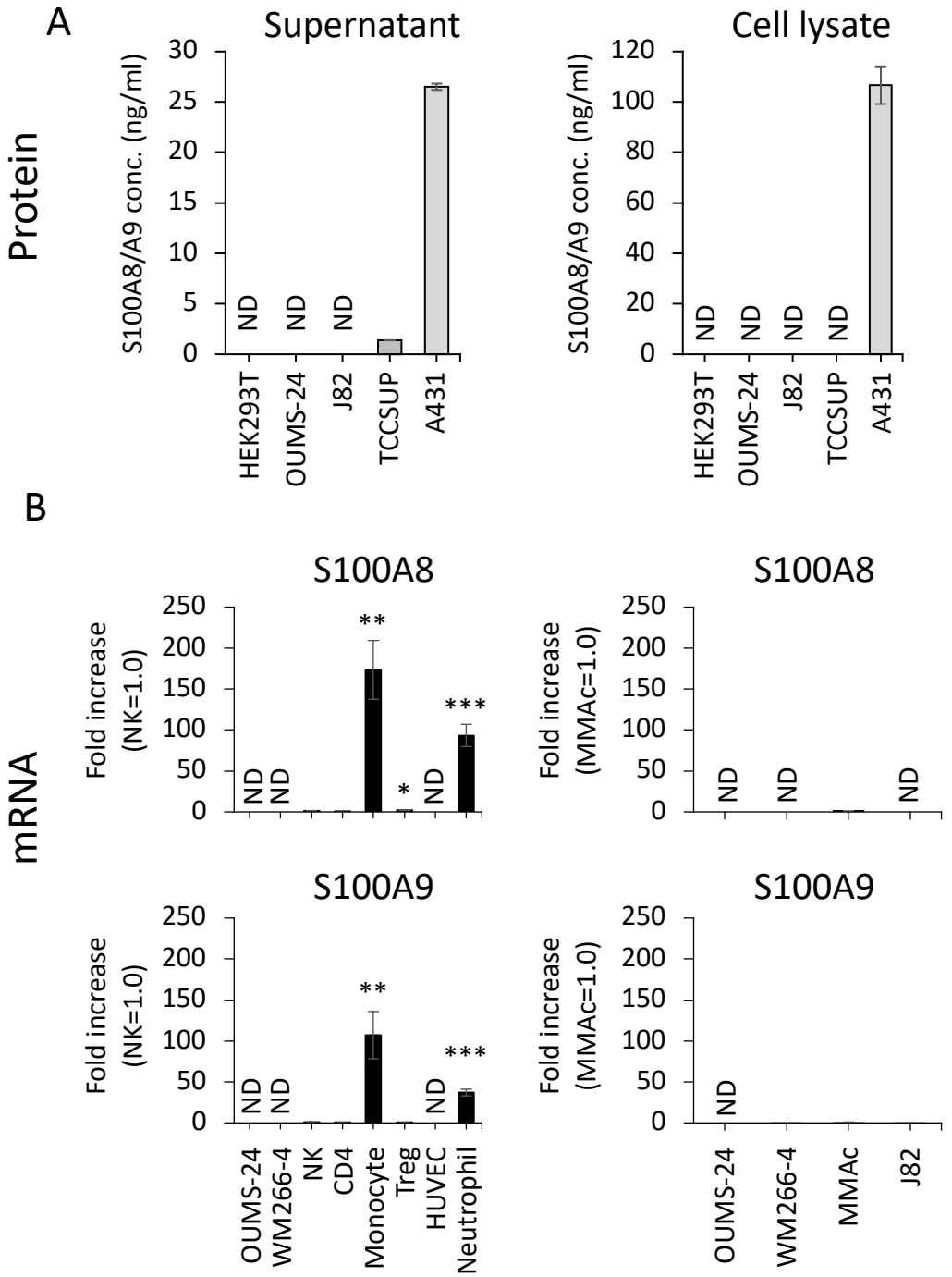

OUMS-24: human fibroblasts

HUVEC: human umbilical vein endothelial cells

Normal

HEK293T: human embryonic kidney epithelial cell line with SV40 large T antigen

Immortal (non-cancer)

J82: human bladder cancer cells

TCCSUP: human bladder cancer cells

A431: human squamous carcinoma cells

WM266-4: human melanoma cells

MMAc: human melanoma cells

Cancer

NK: human NK cells

CD4: human CD4+T cells

Monocyte: human monocytes

Treg: human regulatory T cells

Neutrophil: human neutrophils

Normal

Leukocytes isolated from peripheral blood provided by a healthy donor

Fig. S5. Measurement of S100A8/A9 levels in human cells. A, S100A8/A9 levels in the cultured cells were measured and quantified by a conventional ELISA. Cells and their conditioned media indicated beneath the bar graphs were collected. The collected cell pellets were lysed with M-PER solution (Thermo Fisher Scientific). The collected cell lysates and their corresponding culture media were then subjected to the sandwich ELISA method using our developed S100A8/A9 antibodies (clone #260 was set on the plate and clone #45 conjugated with biotin was used for detection) to monitor the levels of intrinsic S100A8/A9 protein in the specimens. A431 cells were used as a positive control for S100A8/A9 detection; these cells show active production of S100A8/A9 and release of the protein to the extracellular space. B, The indicated leukocytes were collected from the blood specimen of a healthy donor. In brief, leukocytes were separated into two fractions, a mononuclear cell fraction and a polymorphonuclear fraction, by using polymorphprep (Abbot Diagnostics Technologies AS, Oslo, Norway). The monocytes, NK cells, CD4+T cells, and Treg cells were then isolated from the mononuclear cell fraction using CD14 MicroBeads, human (Miltenyi Biotec, Bergisch Gladbach, Germany), an NK Cell Isolation Kit, human (Miltenyi Biotec), CD4 MicroBeads, human (Miltenyi Biotec), and a CD4+CD25+ Regulatory T Cell Isolation Kit, human (Miltenyi Biotec), respectively. On the other hand, neutrophils were isolated from the separated polymorphonuclear fraction using CD16 MicroBeads, human (Miltenyi Biotec) (CD16 positive: neutrophils). Total RNAs prepared from the indicated cells were analyzed for the expression of the S100A8 and S100A9 by RT-qPCR. The amounts of mRNA were calibrated to those of TBP mRNA (internal control) and are presented as the fold increase relative to those of the indicated controls (NK cells (left) and MMAc (right)). Data are means ± SD, *P<0.05, **P<0.01 and ***P<0.001 by Student's *t*-test (n = 3). ND: Not detected.

Rodrigo and Tomonobu et al.

Supplementary Tables

Table. S1

Table S1. Cell lines

Cells		Medium	Source
OUMS-24*	Normal human fibroblasts	DMEM/F12 + 10% FBS (Thermo Fisher Scientific, Waltham, MA)	Dr. Masayoshi Namba
HEK293T	Non-cancerous human embryonic kidney epithelial cell line with stable expression of the simian virus 40 (SV40) large T antigen	DMEM/F12 + 10% FBS (Thermo Fisher Scientific)	RIKEN BioResource Center (Tsukuba, Japan)
HUC	Normal human uroepithelial cells	Urothelial Cell Medium (ScienCell Research Laboratories)	ScienCell Research Laboratories (Carlsbad, CA, USA)
SV-HUC-1	SV40-transformed immortal HUC cells	DMEM/F12 + 10% FBS (Thermo Fisher Scientific)	ATCC (Rockville, MD)
J82	Human urinary bladder transitional carcinoma cell lines	DMEM/F12 + 10% FBS (Thermo Fisher Scientific)	ATCC
TCCSUP	Human urinary bladder transitional carcinoma cell lines	DMEM/F12 + 10% FBS (Thermo Fisher Scientific)	ATCC

* R. Ohashi, M. Miyazaki, K. Fushimi, et al, Enhanced activity of cyclin A-associated kinase in immortalized human fibroblasts, *Int. J. Cancer* 82 (1999) 754-758.

Table. S2

Table S2. Primary antibodies for IHC

Antibody	Commercial source
Rabbit anti-human S100A8 antibody	Santa Cruz Biotechnology, Dallas, TX
Rabbit anti-human S100A9 antibody	Santa Cruz Biotechnology
Mouse anti-human TLR4 antibody	Proteintech, Rosemon, IL
Rabbit anti-human Ki-67 (Ki67)	NeoMarkers, Fremont, CA
Rabbit anti-human collagen type 1 alpha 1 chain (COL1A1)	Cell Signaling Technology, Danvers, MA

Table. S3

Table S3. Primer sequences for RT-qPCR

Target	Forward (5' to 3')	Reverse (5' to 3')
TBP	GAACATCATGGATCAGAACAACA	ATAGGGATTCCGGGAGT
RAGE (AGER)	GGCAGACAGAGCCAGGAC	AGCACCCAGGCTCCAACT
MCAM	CACCGTCCCTGTTTTCTACC	TCCCCTTCCTTCAGCATTC
NPTNα	TCTCGCTGTTGCTGGTCTC	CAGGGCTGTCTCGAATAATGA
NPTNβ	AGGCAAAACCCCTCCATAAC	CAGGGCTGTCTCGAATAATGA
ALCAM	GGCAGTGGAAGCGTCATAA	CATTCTCTTCAGGGGAAATGA
EMMPRIN (BSG)	GAATGACAGCGCCACAGAG	TACTCTCCCCACTGGTCGTC
TLR4	GAACACCAGAGTTTCCTGCAA	TGCCCTGCTTATCTGAAGGT
TAK1 (MAP3K7)	AACTCCATCCCAATGGCTTA	CAATGCTGTTCAAACACTGC
DLK (MAP3K12)	CCATTCCACACCAGGAACTTC	GCATCAACGCTGTTGGAGTTG
TPL2 (MAP3K8)	AGGACCTCCGAGGAACAGA	CCGTCTGCATGTGGATGA
ARAF	TGGTCTACCGACTCATCAAGG	CAAGGACCTCGACAATGAGC
MOS	TTGTGCACTTGGACCTGAAG	AGCACAGCAGATCTTCCAAC

Table. S4

Table S4. Primary antibodies for WB

Antibody	Commercial source
Mouse anti-Myc tag antibody	Cell Signaling Technology
Mouse anti-human TLR4	Santa Cruz Biotechnology
Rabbit anti-human TIRAP	abcam, Cambridge, UK
Rabbit anti-human TPL2	Cell Signaling Technology
Mouse anti-human phospho-MEK1/2 (Ser218/222)	BD Biosciences, Franklin Lakes, NJ
Rabbit anti-human MEK2	Cell Signaling Technology
Rabbit anti-human phospho-p44/42 MAPK (Erk1/2) (Thr202/Tyr204)	Cell Signaling Technology
Rabbit anti-human p44/42 MAPK (Erk1/2)	Cell Signaling Technology
Rabbit anti-human phospho-p38 MAPK (Thr180/Tyr182)	Cell Signaling Technology
Rabbit anti-human p38 MAPK	Cell Signaling Technology
Rabbit anti-human phospho-SAPK/JNK (Thr183/Tyr185)	Cell Signaling Technology
Rabbit anti-human SAPK/JNK	Cell Signaling Technology
Rabbit anti-human phospho-Akt (Ser473)	Cell Signaling Technology
Rabbit anti-human phospho-Akt (Thr308)	Cell Signaling Technology
Rabbit anti-human Akt	Cell Signaling Technology
Mouse anti-β-actin	Sigma-Aldrich, St. Louis, MO